

## Porro 棱镜相位延迟及其补偿波片的设计分析

李之通, 赵一鸣\*, 李祚涵, 庞庆生

北京遥测技术研究所, 北京 100076

**摘要** 利用琼斯矩阵分析了 Porro 棱镜的相位延迟, 并根据相位延迟情况设计了补偿波片。在 Porro 棱镜的最大延时下, 得到两对补偿波片  $0.57\lambda/0.43\lambda$  (对波长为  $\lambda$  的光束产生  $0.57 \times 2\pi/0.43 \times 2\pi$  的相位延迟) 和  $0.93\lambda/0.07\lambda$ 。利用琼斯矩阵仿真了两对波片的补偿情况, 结果表明,  $0.93\lambda/0.07\lambda$  波片能实现补偿的方位角范围为  $3.6^\circ$ , 约为波片  $0.57\lambda/0.43\lambda$  的 3.6 倍, 接近实际实验结果 (3.1 倍)。此外, 较宽的角度调节范围在方便调节激光器的同时能提高激光器的稳定性, 为 Porro 棱镜谐振腔的相位延迟补偿提供了新思路。

**关键词** 激光器; Porro 棱镜; 琼斯矩阵; 相位延迟; 补偿波片

**中图分类号** TN248.1

**文献标志码** A

**doi:** 10.3788/CJL202148.2101004

## 1 引言

正交 Porro 棱镜谐振腔<sup>[1]</sup>在冲击振动条件下具有较强的抗失谐特性, 被广泛应用于航天、军事等领域<sup>[2]</sup>。在星载激光雷达领域, 水星激光测高仪 (MLA) 和地球科学激光高度计 (GLAS) 搭载的激光器在放大级中利用  $0.57\lambda$  (对波长为  $\lambda$  的光束产生  $0.57 \times 2\pi$  的相位延迟) 波片补偿 Porro 棱镜的相位延迟, 实现双通放大输出<sup>[3-4]</sup>。火星轨道激光高度计 (MOLA)、近地小行星会合点 (NEAR)、CLT (Clementine laser transmitter) 搭载的激光器均为正交 Porro 棱镜电光调 Q 单振荡器设计, 在调 Q 臂上用  $0.57\lambda$  波片补偿 Porro 棱镜的退偏, 通过调节输出臂波片的方位角实现可变耦合输出<sup>[5-7]</sup>。云气溶胶激光雷达和红外探路者卫星观测 (CALIPSO) 中搭载的激光器同样采用正交 Porro 棱镜和  $0.57\lambda$  波片补偿的组合, 通过偏振耦合输出 250 mJ 的 1064 nm 基频光<sup>[8]</sup>。

Porro 棱镜的相位延迟与其基底材料有关, Agrawal 等<sup>[9-10]</sup>在正交 Porro 棱镜 Z 型腔中对 BK7、石英和 K9 三种材料进行对比, 利用琼斯矩阵计算出 BK7 和石英材料 Porro 棱镜对应的补偿波片数与方位角的关系, 分析了耦合反射率对脉冲宽

度和单脉冲能量的影响, 并进行了实验验证。利用电矢量末端轨迹也可以计算出不同材料 Porro 棱镜对应的补偿波片数及方位角之间的关系<sup>[11]</sup>。对于石英材料 Porro 棱镜的相位延迟补偿, 普遍采用  $0.57\lambda$  波片, 但在实际操作中, 最佳方位角附近存在与最佳补偿状态接近的方位角, 因此, 调节过程中需要进行仔细判断。此外,  $0.57\lambda$  波片的最佳方位角角度范围较窄, 在一定程度上削弱了 Porro 棱镜的抗失谐能力。

本文针对  $0.57\lambda$  波片调节过程的缺陷, 通过分析石英材料 Porro 棱镜的琼斯矩阵得到一组新的补偿波片  $0.93\lambda/0.07\lambda$ 。该波片的最佳方位角角度范围较宽, 且不存在接近最佳方位角的角度, 在简化调节过程的同时进一步提高了谐振腔的抗失谐能力。实验结果表明,  $0.57\lambda$  波片和  $0.93\lambda$  波片的输出性能一致, 为 Porro 棱镜谐振腔的补偿波片提供了一种新选择。

## 2 Porro 棱镜的相位延迟与补偿波片数分析

光线在 Porro 棱镜内的传输过程如图 1(a) 所示。入射光线在 Porro 棱镜内经过两次全反射产生的相位延迟与棱线的摆放角度  $\beta$  ( $X$  为水平方向,  $Y$

收稿日期: 2021-02-21; 修回日期: 2021-03-22; 录用日期: 2021-04-15

通信作者: \*zym\_bird@126.com

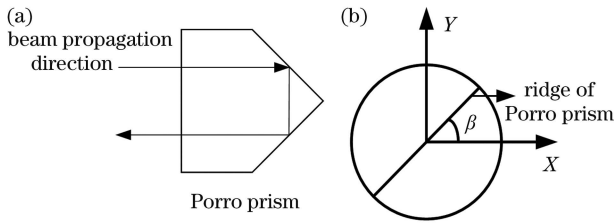


图 1 Porro 棱镜的示意图。(a)全反射示意图;(b)棱线角度示意图

Fig. 1 Schematic diagram of the Porro prism.

(a) Schematic diagram of the total reflection;

(b) schematic diagram of ridge angle

为竖直方向)有关,如图 1(b)所示。在 Porro 棱镜前放置一个偏振片,以检验 Porro 棱镜对线偏振光产生的相位延迟。一束线偏振光经过由 Porro 棱镜和偏振片组成的光学系统的传输过程如图 2 所示。当一束线偏振光(P/S)经 Porro 棱镜全反射后,再次经过偏振片时的有效反射率  $R$  可由琼斯矩阵计算。若有效反射率  $R$  为 0,表明 Porro 棱镜没有对线偏振光产生相位延迟;若  $R$  不为 0,则表明 Porro 棱镜对线偏振光产生了相位延迟。因此,通过有效反射率  $R$  的大小能判断 Porro 棱镜引入的相位延迟大小。

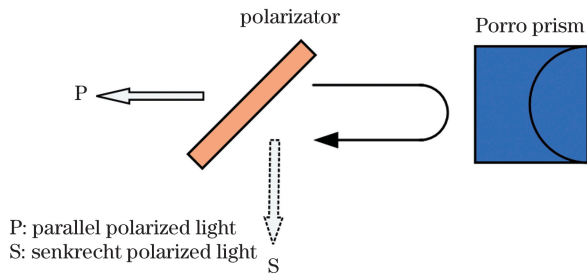


图 2 Porro 棱镜的相位延迟原理

Fig. 2 Principle of phase delay of the Porro prism

设 P 偏振光为水平偏振光,偏振片  $M_P$  可透过 P 偏振光。一束 P 偏振光经过 Porro 棱镜  $M_{Porro}$  全反射后再次经过偏振片  $M_P$  的过程可用琼斯矩阵<sup>[12-13]</sup>表示为

$$M = M_P M_{Porro} H = \begin{bmatrix} \cos(p/2) + i\sin(p/2)\cos(2\beta) \\ 0 \end{bmatrix} = \begin{bmatrix} a + bi \\ 0 \end{bmatrix}, \quad (1)$$

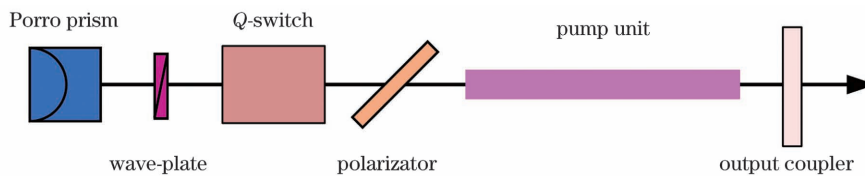


图 4 谐振腔示意图

Fig. 4 Schematic diagram of the resonator

式中,  $M_P = \begin{pmatrix} 1 & 0 \\ 0 & 0 \end{pmatrix}$  为偏振片的琼斯矩阵,  $M_{Porro} = \begin{pmatrix} A & B \\ B & A^* \end{pmatrix}$  为 Porro 棱镜的琼斯矩阵,  $H = \begin{pmatrix} 1 \\ 0 \end{pmatrix}$  为 P 偏振光的琼斯矩阵。其中,  $A = \cos(p/2) + i\sin(p/2)\cos(2\beta)$ ,  $A^*$  为  $A$  的复共轭,  $B = i\sin(p/2)\sin(2\beta)$ ,  $p = \pi + 4\arctan\{[\cos\alpha \times (\sin^2\alpha - n^{-2})^{1/2}]/\sin^2\alpha\}$  为 Porro 棱镜内产生的相移角度,  $\alpha = 45^\circ$  为光的入射角度,  $n = 1.45$  为石英 Porro 棱镜的折射率。

偏振片的有效反射率  $R$  可表示为<sup>[1]</sup>

$$R = 1 - (a^2 + b^2) - [\cos^2(p/2) + \sin^2(p/2)\cos^2(2\beta)]. \quad (2)$$

根据(2)式得到偏振片有效反射率  $R$  随棱线角度的变化关系,结果如图 3 所示。可以发现,当  $\beta = 45^\circ/135^\circ$  时,反射率最大,表明此时 Porro 棱镜产生的相位延迟最大。

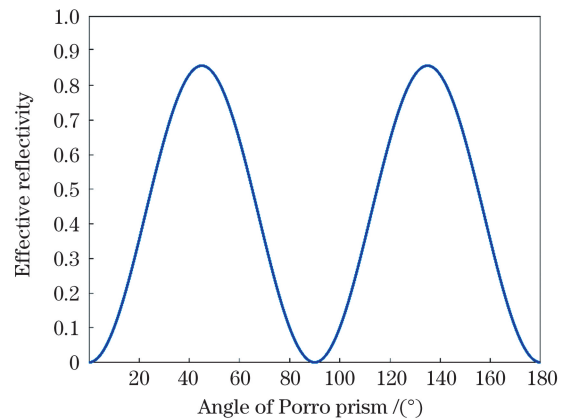


图 3  $R$  与 Porro 棱镜棱线角度的关系

Fig. 3 Relationship between  $R$  and ridge angle of the Porro prism

Porro 棱镜的抗失谐特性只体现在与棱线垂直的方向上,即棱线沿 X/Y 方向放置时只能保证入射光线在 Y/X 方向的抗失谐特性。当棱线角度  $\beta = 45^\circ/135^\circ$  时,可以同时提高 X 和 Y 方向的稳定性,因此,选取图 4 中的谐振腔模型,采用升压调 Q 方式分析  $\beta = 45^\circ/135^\circ$  时 Porro 棱镜的补偿情况。由于 Porro 棱镜会引入相位延迟,当 Q 开关未加电压

且腔内波片为  $\lambda/4$  波片时,调节  $\lambda/4$  波片的方位角不能使谐振腔处于低  $Q$  状态,即不能实现谐振腔的调  $Q$  运转。因此,需要在墙内插入特殊的波片,以实现谐振腔的调  $Q$  运转。

未加电压情况下,假设腔内为 P 偏振光,经过波片、Porro 棱镜、波片组成的光学系统后,该偏振光的琼斯矩阵可表示为

$$M = M_p M_{wp} M_{Porro} M_{wp} H, \quad (3)$$

式中,  $M_{wp} = \begin{pmatrix} C & D \\ D & C^* \end{pmatrix}$  为波片的琼斯矩阵,其中,  $C = \cos(\varphi/2) + i\sin(\varphi/2) \cos(2\delta)$ ,  $D = i\sin(\varphi/2) \sin(2\delta)$ ,  $C^*$  为矩阵中  $C$  的复共轭,  $\varphi$  为波片引起的相移角度,  $\delta$  为波片旋转的方位角。简化后得到

$$M = \begin{pmatrix} AC^2 + 2BCD + A^* D^2 & \\ 0 & 0 \end{pmatrix} = \begin{pmatrix} c + di & \\ & 0 \end{pmatrix}, \quad (4)$$

式中,  $c$ 、 $d$  均为实数,  $c$  为元素  $AC^2 + 2BCD + A^* D^2$  的实部,  $di$  为元素  $AC^2 + 2BCD + A^* D^2$  的虚部。偏振片的有效反射率  $R = 1 - (c^2 + d^2)$ ,为了保证谐振腔处于低  $Q$  值状态,要求  $R = 1$ ,求解出满足条件的波片为  $0.57\lambda/0.43\lambda$  和  $0.93\lambda/0.07\lambda$ 。 $0.57\lambda/0.43\lambda$  和  $0.93\lambda/0.07\lambda$  为两组互补波片,每组内的两种波片状态相同。因此,选取  $0.57\lambda$  和  $0.93\lambda$  波片进行分析,得到偏振片的有效反射率与两种波片方位角的关系,如图 5 所示。

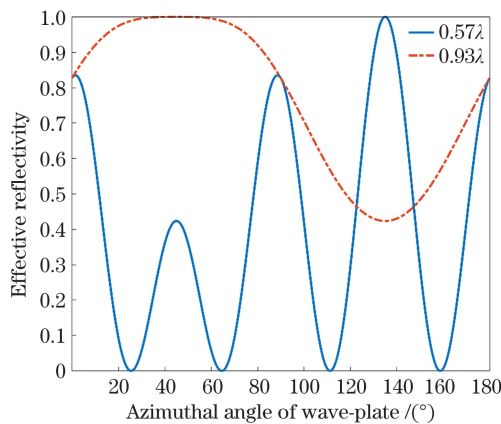


图 5 偏振片有效反射率与不同波片方位角的关系  
Fig. 5 Relationship between azimuthal angle of different wave-plate and effective reflectivity

从图 5 可以发现,方位角为  $0^\circ \sim 180^\circ$  时,波片的有效反射率呈周期变化,  $0.57\lambda$  波片的方位角在  $134.92^\circ \sim 135.08^\circ$  范围时,偏振片的有效反射率可以达到 1,最大反射率处的曲线比较尖锐;  $0.93\lambda$  波片的方位角在  $43.12^\circ \sim 46.88^\circ$  范围时,偏振片的有效反射率可以达到 1,最大反射率处的曲线比较平

缓,调节范围更宽。此外,  $0^\circ \sim 180^\circ$  范围内,  $0.57\lambda$  波片存在 4 个高反射率峰,其中, 3 个峰的有效反射率都超过 80%,只有 1 个峰的有效反射率为 1,因此在调节过程中就需要判断波片的最佳方位角。  $0.93\lambda$  波片只存在 1 个高反射率的峰,在调节过程中更容易判断出谐振腔低  $Q$  值的最佳波片方位角。

### 3 实验结果

在图 4 所示的谐振腔中,依据图 5 中两种波片方位角与偏振反射率的关系进行实验验证。实验中的增益介质为 1% 掺杂的 Nd:YAG 晶体,尺寸为  $6\text{ mm} \times 6\text{ mm} \times 130\text{ mm}$ ,采用侧面泵浦方式,泵浦光的频率为 20 Hz,脉冲宽度为  $145\ \mu\text{s}$ ,石英材料 Porro 棱镜呈棱线  $45^\circ$  放置,用  $\text{KD}^* \text{P}$  作为光电调  $Q$  晶体,用升压调  $Q$  方式输出。将波片安装在带有角度刻度的调整架中,在自由运转条件下,通过增加泵浦电流和旋转波片的方式,寻找最大泵浦电流下使谐振腔处于低  $Q$  状态的最佳波片方位角范围,实验结果如表 1 所示。可以发现,相同泵浦功率条件下,谐振腔处于低  $Q$  状态时,  $0.93\lambda$  波片的调节范围大于  $0.57\lambda$  波片。

表 1 低  $Q$  状态下不同波片的调节范围

Table 1 Adjustment ranges of different wave-plate in low- $Q$  state

Wave-plate	Adjustment angle / ( $^\circ$ )
$0.57\lambda$	$\sim 2.2$
$0.93\lambda$	$\sim 6.8$

由图 5 可知,  $0.57\lambda$  波片中有 3 个峰可使有效反射率超过 80%,但只有 1 个峰能达到 100%,在实际调节中需要通过增大泵浦逐一判断波片的最佳方位角。而  $0.93\lambda$  波片只存在 1 个峰,调节过程更方便。图 6、图 7 为两种波片的输出情况,可以发现,

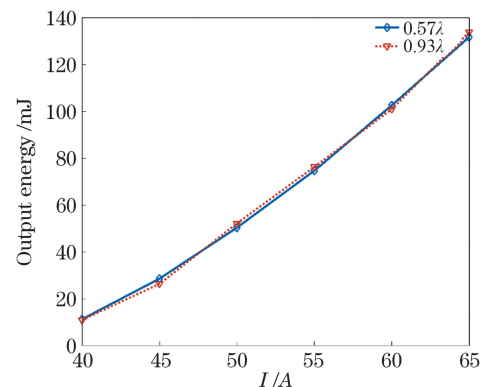


图 6 两种波片的谐振腔输出能量

Fig. 6 Output energy of two wave-plates

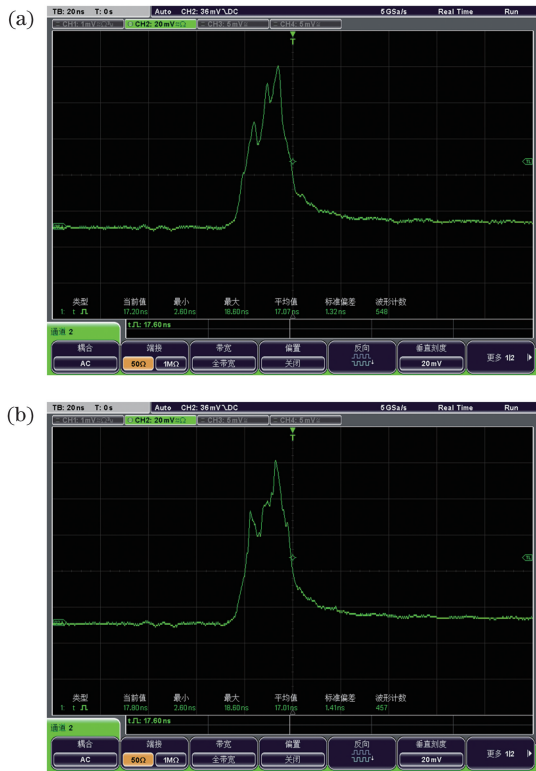


图 7 两种波片谐振腔的脉冲宽度。(a)  $0.57\lambda$ ; (b)  $0.93\lambda$

Fig. 7 Pulse width of two wave-plate resonators.

(a)  $0.57\lambda$ ; (b)  $0.93\lambda$

在调 Q 驱动电压相同的条件下,两种波片在各自调节范围内谐振腔输出的能量及脉冲宽度基本一致。

## 4 结 论

分析了石英材质 Porro 棱镜引入的相位延迟,利用琼斯矩阵计算出 Porro 棱镜棱线角度  $\beta=45^\circ/135^\circ$  时,能够补偿其相位延时的波片为  $0.57\lambda/0.43\lambda$ 、 $0.93\lambda/0.07\lambda$ 。由于两组波片为互补的波片,将  $0.93\lambda$  波片与常用的  $0.57\lambda$  波片进行了理论分析和实验验证,结果表明,在单 Porro 调 Q 激光器中谐振腔处于低 Q 值状态时, $0.93\lambda$  波片的调节范围约为  $6.8^\circ$ ,是  $0.57\lambda$  波片的 3.1 倍,该结果与理论分析的结论(3.6 倍)基本一致,且更宽的角度范围有助于提高谐振腔的抗失谐能力。在理论分析中, $0.57\lambda$  波片存在多个使谐振腔接近低 Q 值状态的方位角角度,在调节过程中需将其与真正低 Q 值的角度位置进行区分,而  $0.93\lambda$  波片只存在一处使谐振腔处于低 Q 状态的位置。实验中, $0.57\lambda$  波片的最佳方位角角度需要通过增加泵浦功率对多个接近低 Q 值状态的角度逐一进行验证,而  $0.93\lambda$  波片只有一处能使谐振腔处于低 Q 状态,调节过程更简单,为 Porro 棱镜的补偿波片提供了新的选择,也为

进一步提高激光器谐振腔的稳定性提供了思路。

## 参 考 文 献

- [1] Chun M K, Teppo E A. Laser resonator: an electrooptically Q-switched Porro prism device [J]. Applied Optics, 1976, 15(8): 1942-1946.
- [2] Agrawal L, Bhardwaj A, Pal S, et al. Resonator design and performance estimation for a space-based laser transmitter [J]. Proceedings of SPIE, 2006, 6409: 64091E.
- [3] Krebs D J, Novo-Gradac A M, Li S X, et al. Compact, passively Q-switched Nd:YAG laser for the MESSENGER mission to Mercury [J]. Applied Optics, 2005, 44(9): 1715-1718.
- [4] Afzal R S. Performance of the GLAS laser transmitter [J]. Proceedings of SPIE, 2006, 6100: 610020.
- [5] Afzal R S. Mars observer laser altimeter: laser transmitter [J]. Applied Optics, 1994, 33(15): 3184-3188.
- [6] Cole T D. NEAR laser rangefinder: a tool for the mapping and topologic study of asteroid 433 eros [J]. Johns Hopkins Apl Technical Digest, 1998, 19(2): 142-157.
- [7] Kushina M E, Grote M G, Wiswall C E, et al. Clementine: diode-pumped laser qualification [J]. Proceedings of SPIE, 1995, 2379: 137-140.
- [8] Hovis F E. Qualification of the laser transmitter for the CALIPSO aerosol lidar mission [J]. Proceedings of SPIE, 2006, 6100: 61001X.
- [9] Agrawal L, Bhardwaj A, Pal S, et al. Jones matrix formulation of a Porro prism laser resonator with waveplates: theoretical and experimental analysis [J]. Applied Physics B, 2007, 89(2/3): 349-357.
- [10] Shen J P, Ding C F. Characteristic analysis of Z-shaped orthogonal Porro-prism resonator [J]. Laser & Infrared, 2012, 42(3): 283-287.  
沈建平, 丁春峰. Z 型正交波罗棱镜腔的特性研究 [J]. 激光与红外, 2012, 42(3): 283-287.
- [11] Luo X, Wang P F. Research on polarization coupling output characteristics of Porro prism cavity [J]. Laser & Infrared, 2016, 46(10): 1244-1249.  
罗旭, 王鹏飞. 直角棱镜腔偏振耦合输出特性研究 [J]. 激光与红外, 2016, 46(10): 1244-1249.
- [12] Gil J, Bernabeu E. Obtainment of the polarizing and retardation parameters of a non-depolarizing optical system from the polar decomposition of its Mueller matrix [J]. Optik, 1986, 76(2): 67-71.
- [13] Lu Y X, Lü B D. Matrix optics [M]. Dalian: Dalian University of Technology Press, 1989: 323-338.  
卢亚雄, 吕百达. 矩阵光学 [M]. 大连: 大连理工大学出版社, 1989: 323-338.

# Design and Analysis of Phase Delay of Porro Prism and Compensation Wave-Plate

Li Zhitong, Zhao Yiming<sup>\*</sup>, Li Zuohan, Pang Qingsheng

*Beijing Research Institute of Telemetry, Beijing 100076, China*

**Abstract** The orthogonal Porro prism resonant cavity has strong anti-detuning characteristics under shock vibration conditions, so it has a wide range of applications in the military and aerospace fields. The ridge line is typically set at  $45^\circ$  when using Porro prisms. A wave plate must be added to compensate for the phase delay introduced by the Porro prism. Quartz Porro prisms are generally compensated by  $0.57\lambda$  wave-plates (where  $\lambda$  is the wavelength of light). In practice, the optimal compensation azimuth angle range of  $0.57\lambda$  wave-plates is relatively narrow, and there are numerous azimuths near the wave-plate's best azimuth angle. Therefore, it is equivalent to weakening the anti-detuning ability of the Porro prism. This study reported that a  $0.93\lambda$  wave-plate could compensate for the phase retardation of Porro prisms. The  $0.93\lambda$  wave-plate has a wide optimal compensation range angle, and no angle is close to the optimal compensation range angle. It provides new ideas for the phase delay compensation of Porro prisms.

**Objective** In the optical system shown in Fig. 2, the effective reflectivity of the polarizer is calculated by using the Jones matrix and the relationship between the phase delay of the Porro prisms for linearly polarized light and the Porro ridge angle are analyzed. The resonant cavity shown in Fig. 4, the Porro prism ridge line, is placed at  $45^\circ/135^\circ$ , and the resonant cavity is at a low- $Q$  state when the  $Q$ -switch is without high voltage. It is calculated by Jones matrix that two groups of  $0.57\lambda/0.43\lambda$  and  $0.93\lambda/0.07\lambda$  can make the resonant cavity in a low- $Q$  state. Since the two wave plates in each group of wave-plates are complementary, the  $0.57\lambda$  and  $0.93\lambda$  wave-plates are selected for theoretical analysis and experimental comparison. The Jones matrix is used to perform the theoretical simulation of the compensation of the two wave-plates, and the experimental verification is performed in the resonant cavity shown in Fig. 4 based on the hypothetical simulation results. The wave-plate is installed in an adjustable frame with an adjustable angle in the experiment. Under free-running conditions, the wave-plate is rotated while increasing the pumping current to determine the best azimuth angle range for the resonant to be in a low- $Q$  state at the maximum pumping current.

**Results and Discussions** In the optical system shown in Fig. 2, the phase delay produced by Porro prism is demonstrated in Fig. 3 when the ridge angle is  $45^\circ/135^\circ$ , the effective reflectivity of the polarizer is the largest indicating that the Porro prism produces the largest phase delay at these angles. The Porro prism ridge line angle in the resonant cavity shown in Fig. 4 is  $45^\circ/135^\circ$ . According to the Jones matrix simulation results, the  $0.57\lambda$  and  $0.93\lambda$  wave-plates can make the cavity in a low- $Q$  state; at this state, the azimuth angle range of the  $0.93\lambda$  wave-plate is  $3.6^\circ$ , which is about 3.6 times that of the  $0.57\lambda$ , as shown in Fig. 5. It can also be seen in Fig. 5 that the  $0.93\lambda$  wave-plate does not have any other angles that are close to the optimal compensation angle within the adjustment range of  $0^\circ-180^\circ$ . The  $0.57\lambda$  wave-plate, however, has multiple angles that are close to the optimal compensation angle. The experimental verification, according to the theoretical analysis, shows that the adjustment range of the  $0.93\lambda$  wave-plate in the low- $Q$  state of the resonator is about  $6.8^\circ$ , and the adjustment range of the  $0.57\lambda$  wave-plate is about  $2.2^\circ$ , as shown in Table 1. The optimal adjustment range of the  $0.93\lambda$  wave-plate is about 3.1 times that of the  $0.57\lambda$  waveplate, which is consistent with the theoretical results. In addition, the output laser parameters of the two kinds of wave-plates are compared, and the results of the energy and pulse width of the two are the same, shown in Fig. 6 and Fig. 7.

**Conclusions** This paper analyzes the phase delay introduced by the Porro prism made of quartz, the number of wave-plates that can compensate the phase delay is calculated using Jones matrix:  $0.57\lambda/0.43\lambda$  and  $0.93\lambda/0.07\lambda$ . Since the two sets of wave-plates are complementary wave plates, the  $0.93\lambda$  wave-plate and commonly used  $0.57\lambda$  wave-plate have been theoretically analyzed and verified by experiments. The results show that the adjustment range of the  $0.93\lambda$  wave-plate is about  $6.8^\circ$  to make the resonant cavity in a low- $Q$  state, which is 3.1 times that of the  $0.57\lambda$  wave-plate. The result is consistent with that of the theoretical analysis. In the theoretical analysis, the  $0.57\lambda$  wave-plate has multiple azimuth angles that make the resonant cavity close to the low- $Q$  state, whereas the

$0.93\lambda$  wave-plate has only one azimuth angle. This result has been experimentally verified. In the actual adjustment process, determining the best azimuth angle of the  $0.57\lambda$  wave-plate one by one is necessary, and the  $0.93\lambda$  wave plate is more convenient. Compared with the  $0.57\lambda$  wave-plate, the  $0.93\lambda$  wave-plate has a wider range of optimal angles when compensating the phase delay of the Porro prism, and the adjustment is more convenient. This provides a new choice for the Porro prism compensation wave-plate and ideas for further improving the stability of the laser cavity.

**Key words** lasers; Porro prism; Jones matrix; phase delay; compensation wave-plate

**OCIS codes** 140.3410; 140.3460; 140.3480